Title

Ultrasensitive and rapid detection of ochratoxin A in agro-products by a nanobody-mediated FRET-based immunosensor

Authors

Tang, Zongwen
Liu, Xing
Su, Benchao
et al.

Publication Date

2020-04-01

DOI

10.1016/j.jhazmat.2019.121678

Peer reviewed

HHS Public Access

Author manuscript

J Hazard Mater. Author manuscript; available in PMC 2021 April 05.

Published in final edited form as:

J Hazard Mater. 2020 April 05; 387: 121678. doi:10.1016/j.jhazmat.2019.121678.

Ultrasensitive and rapid detection of ochratoxin A in agro-products by a nanobody-mediated FRET-based immunosensor

Zongwen Tang[a,1], **Xing Liu**[a,1,*], **Benchao Su**[a,1], **Qi Chen**[a], **Hongmei Cao**[a], **Yonghuan Yun**[a], **Yang Xu**[b], **Bruce D. Hammock**[c]

[a]College of Food Science and Engineering, Hainan University, 58 Renmin Avenue, Haikou 570228, PR China

[b]State Key Laboratory of Food Science and Technology, Nanchang University, 235 Nanjing East Road, Nanchang, 330047, PR China

[c]Department of Entomology and Nematology and UCD Comprehensive Cancer Center, University of California, Davis, CA, 95616, United States

Abstract

Ochratoxin A (OTA) is a major concern for public health and the rapid detection of trace OTA in food is always a challenge. To minimize OTA exposure to consumers, a nanobody (Nb)-mediated förster resonance energy transfer (FRET)-based immunosensor using quantum dots (Nb-FRET immunosensor) was proposed for ultrasensitive, single-step and competitive detection of OTA in agro-products at present work. QDs of two sizes were covalently labeled with OTA and Nb, acting as the energy donor and acceptor, respectively. The free OTA competed with the donor to bind to acceptor, thus the FRET efficiency increased with the decrease of OTA concentration. The single-step assay could be finished in 5 min with a limit of detection of 5 pg/mL, which was attributed to the small size of Nb for shortening the effective FRET distance and improving the FRET efficiency. The Nb-FRET immunosensor exhibited high selectivity for OTA. Moreover, acceptable accuracy and precision were obtained in the analysis of cereals and confirmed by the liquid chromatography-tandem mass spectrometry. Thus the developed Nb-FRET immunosensor was demonstrated to be an efficient tool for ultrasensitive and rapid detection of OTA in cereals and provides a detection model for other toxic small molecules in food and environment.

Graphical Abstract

[*]Corresponding Author: Tel./Fax: +86-898-66193581, xliu@hainanu.edu.cn (X.L.).

[1]These authors contributed equally to this work

Declarations of interest: none.

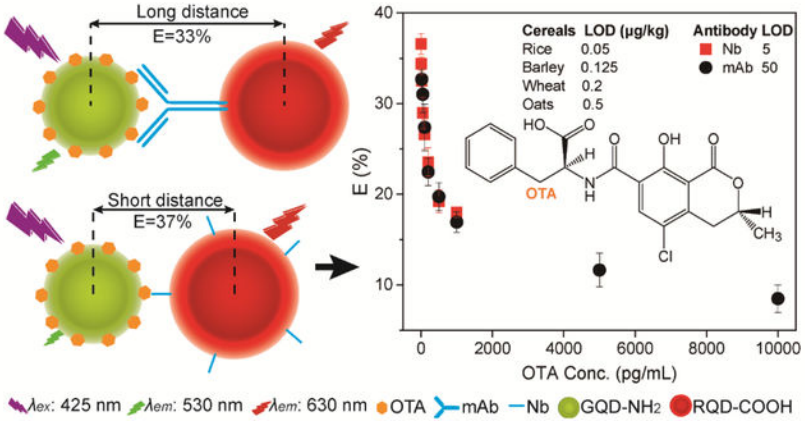

Keywords

Nanobody; quantum dots; immunosensor; förster resonance energy transfer; mycotoxin

1. Introduction

Ochratoxin A (OTA) is a mycotoxin mainly produced by *Aspergillus* and *Penicillium* species through secondary metabolism (Binder, 2007). OTA has been confirmed to be nephrotoxic, hepatotoxic, carcinogenic and teratogenic for animals (Damiano et al., 2018; Shin et al., 2019; Stoev, 2010; Woo et al., 2012). The International Agency for Research on Cancer cataloged OTA in group 2B as a human possible carcinogen (IARC, 1993). OTA is a major concern around the world not only for its severe threat on human health but also for the economic losses from contaminated agro-products. The occurrence of OTA is widespread in coffee, beans, meats, milk, eggs, grapes, cereals, and cereal products, which could be harmful to consumers for its toxic effects (Heussner and Bingle, 2015). The maximum permitted levels of OTA in food have been defined by nations and organizations to ensure public health and safety. Typically, the European Union has set the maximum residue limit of OTA as 10 μg/kg in soluble coffee, 2 μg/kg in wine, 0.5 μg/kg in baby food, 5 μg/kg in cereal, and 3 μg/kg in cereal products, respectively (Commission of the European Communities, 2006). Therefore, it is essential to develop highly sensitive methods for assisting regulation and minimizing exposure to OTA.

Chromatography methods are routinely used for the detection of OTA because of high sensitivity and reliability, such as high-performance liquid chromatography, liquid chromatography-mass spectrometry, gas chromatography-mass spectrometry, and liquid chromatography-tandem mass spectrometry (LC-MS/MS) (Öncü et al., 2019; Rodríguez-Cabo et al., 2016; Wei et al., 2018; Zhang et al., 2019). These methods are adopted as the standard protocols but not suitable for rapid and on-site analysis of OTA. Immunoassays are selected as the alternative methods to detect OTA for ease of operation, good selectivity, and high-throughput screening. Various kinds of immunoassays have been developed for OTA and other analytes, such as enzyme-linked immunosorbent assay, immunosensor, fluorescence immunoassay, chemiluminescence immunoassay and bioluminescence

immunoassay (Dong et al., 2019; Liu et al., 2017; Pagkali et al., 2018; Pagkali et al., 2017; Ren et al., 2019; Sun et al., 2018; Zangheri et al., 2015). Immunosensor integrates advantages of both immunoassay and biosensor, including speediness, high sensitivity and precision, making it a promising tool for food and environment analysis. Heterogeneous immunosensors require repetitive incubation, separation and washing steps, which are error-prone and cause weak binding reactions along with the decrease of sensitivity (Takkinen and Žvirblienė, 2019). In contrast, the homogeneous methods simplify the procedures into mixing of the sample and immune reagents followed by detection, which could shorten assay time, eliminate signal variations from multiple separation and washing steps, and improve detection sensitivity (Ullman, 2013). Various immunosensors have been developed for homogeneous detection of large and small molecules, such as electrochemical immunosensor, luminescent immunosensor, and fluorescent immunosensor (Bhatnagar et al., 2016; Jo et al., 2016; Qian et al., 2017). Förster resonance energy transfer (FRET), referring to the transmission of photoexcitation energy from a donor molecule to a nearby acceptor molecule, is a widely used strategy for homogeneous immunodetection (Masters, 2014). Generally, both antibody and antigen molecules are labeled with fluorescence materials serving as the energy donor and acceptor in FRET-based immunosensor, such as organic dyes and gold nanoparticles. In most recent years, quantum dots (QDs) have been attractive as an efficient fluorescent label in biosensors for exceptional brightness, high photostability, ease of modification, size-adjustable spectrum, wide excitation spectrum, and large surface area to volume ratio (Nsibande and Forbes, 2016; Xu et al., 2016; Zhou et al., 2018). QDs have been demonstrated to be simultaneously effective as the donor and acceptor in FRET, and the FRET-based immunosensors using QDs of two sizes show robust performance on highly sensitive detection of both large and small molecules with an ideal energy transfer efficiency (Chen et al., 2006; Vinayaka and Thakur, 2013). Föster's theory indicates that the energy transfer efficiency inversely correlates to the sixth power of the distance between the donor and acceptor, namely effective FRET distance (Lakowicz, 1999). The monoclonal antibodies (mAbs) are widely adopted in the reported FRET-based immunosensors using QDs for small molecules (Bhatnagar et al., 2016; Xu et al., 2014). Therefore, the substitution of the mAb with a miniaturized antibody could contribute to shorten the effective FRET distance and improve the energy transfer efficiency for higher detection sensitivity.

Miniaturized antibodies are generated by reserving the antigen recognition sites of intact antibodies through genetic engineering technology and digestion with papain and pepsin (Nelson, 2010). Numerous kinds of miniaturized antibodies have been developed, such as the single-chain variable fragment, antigen-binding fragment (Fab), $F(ab')_2$ fragment, single-domain antibodies (sdAbs). Among those miniaturized antibodies, the nanobody (Nb), an sdAb from the heavy chain-only antibody (HCAb) devoid of light chains that occurs naturally in Camelidae, has attracted widespread attention (Muyldermans, 2013). The Nb is also known as VHH, which refers to the variable domain of the heavy chain of HCAbs. Compared to the rest mniaturized antibodies, Nb shows characteristics of the nanoscale cylindrical shape (2.5 nm diameter and 4 nm height), ease of production by prokaryotic expression system, high tolerance to harsh environment, good water solubility, and ease of gene manipulation (Harmsen and De Haard, 2007; Liu et al., 2017; Vincke and

Muyldermans, 2012). Numerous Nbs have been produced against various small and large molecules, including mycotoxins, pestcides, foodborne pathogens and other contaminants in food and environment (He et al., 2018; Liu et al., 2014; Qiu et al., 2018; Tu et al., 2016; Wang et al., 2014; Wang et al., 2015; Wang et al., 2019a; Wang et al., 2019b). As the reported smallest antigen-binding domain, the Nb could be an efficient tool for shortening the effective FRET distance (Qiu et al., 2016; Tang et al., 2019). Nevertheless, a FRET-based immunosensor using an Nb for competitive homogeneous detection of OTA and other small molecules has not yet been reported.

HCAbs against OTA have been raised in an alpaca and the Nbs have been cloned and identified in our previous work (Liu et al., 2014). Among those Nbs, the Nb28 shows the best performance in sensitivity and affinity and has been applied to various formats of immunoassays (Liu et al., 2017; Sun et al., 2019; Sun et al., 2018; Sun et al., 2017; Tang et al., 2019; Tang et al., 2018). In this work, we set about the construction of a FRET-based immunosensor using Nb28 and QDs of two sizes for homogeneous and competitive detection of OTA. The optimization of experiment parameters was described in detail. Based on the optimal conditions, the performance of Nb- and mAb-mediated FRET-based immunosensor was compared. Moreover, the constructed immunosensor was applied to the analysis of OTA in cereal samples and validated by the LC-MS/MS method.

2. Materials and methods

2.1 Materials and instruments

N-hydroxysuccinimide (NHS), N-hydroxysulfosuccinimide (NHSS), N,N-dimethylformamide (DMF), N-(3-dimethylaminopropyl)-N′-ethylcarbodiimide hydrochloride (EDC), N,N-dicyclohexylcarbodiimide (DCC), glucosamine hydrochloride, and gluconic acid were purchased from Aladdin Chemistry Co., Ltd. (Shanghai, China). Ochratoxin A, ochratoxin C (OTC), and fumonisin B_1 (FB_1) were obtained from Pribolab (Singapore). Aflatoxin B_1 (AFB_1) and zearalenone (ZEN) were purchased from Fermentek (Jerusalem, Israel). Ochratoxin B (OTB) was from Bioaustralis (Smithfield, NSW, Australia). Deoxynivalenol (DON) was from Sigma-Aldrich (CA, USA). The 0.45 μm syringe filter was obtained from Xingya Inc. (Shanghai, China). The mouse anti-OTA monoclonal antibody mAb YK232 was obtained from Yikang Biotech Inc. (Haikou, China). The opaque black polystyrene 96-well microtiter plates were purchased from Costar (Corning, USA). Stock solutions (8.01 μM in 50 mM borate buffer, pH 8.4) of the carboxylic acid-modified ZnCdSe/ZnS quantum dots with maximum emission wavelength at 625 nm (RQD-COOH) and the amino group-modified ZnCdSe/ZnS quantum dots with maximum emission wavelength at 525 nm (GQD-NH_2) were purchased from Jiayuan Tech. Co., Ltd. (Wuhan, China). All other chemicals and organic solvents were of reagent grade or better.

Fluorescence spectra and UV–vis spectra were obtained using a spectral scanning multimode reader (Infinite M200 pro, Tecan Ltd., Männedorf, Switzerland). JEM 2100 Transmission electron microscope (JEOL Ltd., Tokyo, Japan) was used for the morphology analysis of the Nb-mediated FRET-based immunosensor. Fourier transform infrared spectroscopy (FTIR) spectra were measured using a TENSOR27 TGA-IR spectrometer

(Bruker Ltd., Karlsruhe, Germany) within the range of 4000–400 cm^{-1} (resolution set as 4 cm^{-1}).

2.2 Preparation of OTA-labeled GQD conjugates

The amino group-modified QDs were covalently coupled to the carboxyl group on OTA by the DCC/NHS method (Xu et al., 2014). Briefly, 100 μL of DMF solution containing 6.4 nmol DCC and 3.2 nmol NHS was mixed with the standard solutions of 0.8, 1.6 and 3.2 nmol OTA, respectively. The mixture was shaken at 30 °C for 120 min to prepare the active esters of OTA. The final solution containing ester-activated OTA was dropwise added to 500 μL of GQD-NH_2 solution (0.4 μM in 0.2 M pH 7.4 borate buffer). The mixture was vigorously shaken at room temperature for 90 min, followed by adding 0.2 μmol ester-activated gluconic acid prepared as described above to block the excess amino groups of GQD for 60 min. The OTA-labeled GQD conjugates (OTA-GQDs) were obtained after twice centrifugation (27000 ×g, 30 min) at 4 °C, and the residual OTA in the supernatant was quantitatively determined by an indirect competitive ELISA as described previously (Liu et al., 2017). The OTA-GQDs were resuspended with 500 μL of borate buffer (0.2 M, pH 7.4) and stored at 4 °C until use. The OTA-GQDs and free GQD-NH_2 were characterized by UV–vis absorption, fluorescence spectra, TEM, and FTIR.

2.3 Preparation of Nb-labeled RQD conjugates

The nanobody Nb28 (10 mg/mL) was expressed and purified as described previously (Tang et al., 2019). The Nb28-labeled RQD was prepared using the EDC/NHSS method (Xu et al., 2014). Briefly, 2 nmol EDC, 5 nmol NHSS, and 0.2 nmol RQD-COOH were added to 500 μL of borate buffer (0.05 M, pH 5.0) and gently mixed at 30 °C for 30 min. The Nb28 solution was added to the ester-activated RQD solution with pH adjusted to 7.4 and incubated at room temperature for 30 min. After blocking with 0.2 μmol glucosamine hydrochloride by stirring for 60 min, the Nb28-labeled RQD conjugates (Nb-RQDs) were separated as described for OTA-GQDs. The residual content of Nb28 in the supernatant was determined by a NanoDrop 1000. The collected Nb-RQDs were dissolved in borate buffer (0.2 M, pH 7.4) and stored at 4 °C prior to use. The Nb-RQDs were characterized by UV–vis absorption, fluorescence spectra, TEM, and FTIR by comparison with free RQD-COOH.

2.4 Procedure of Nb-mediated FRET-based immunosensor

The Nb-mediated FRET-based immunosensor (Nb-FRET immunosensor) was performed as follows. Briefly, 10 μL of OTA-GQDs (donor), 40 μL of Nb-RQDs (acceptor), and 130 μL of borate buffer (0.06 M, pH 7.8) containing 20 mM sodium chloride were added into the wells of a black microtiter plate. Then 20 μL of OTA standard solution with various concentrations (0, 0.005, 0.01, 0.02, 0.05, 0.1, 0.2, 0.5 and 1.0 ng/mL in borate buffer containing 50% methanol) was added into the wells. After incubation at 37 °C for 10 min, the fluorescence intensity (FI) at 530 nm of the mixture caused by FRET between OTA-GQDs and Nb-RQDs was recorded (λ_{ex}: 425 nm). The quantitative analysis of OTA was performed using the standard curve that was constructed by plotting the energy transfer efficiency (E) against the logarithm of OTA concentrations. The E value was calculated according to the equation: $E = (FI_0\text{-}FI)/FI_0$, where FI_0 and FI are the fluorescence intensity at 530 nm at the absence and presence of acceptor.

2.5 Selectivity of the Nb-mediated FRET-based immunosensor

In order to evaluate the selectivity of Nb-FRET immunosensor, cross-reactivities (CRs) of six substitutes of OTA (OTB, OTC, AFB_1, ZEN, FB_1, and DON) with two concentrations (0.1 and 1 ng/mL) were tested. The CR equals to the value of (IC_{50} of OTA/IC_{50} of the tested substitutes)] × 100, where the IC_{50} is defined as the analyte concentration that yields 50% inhibition of QD binding (Guo et al., 2018).

2.6 Sample preparation and analysis

Four cereal samples (rice, oats, barley, and wheat) were prepared for the Nb-FRET immunosensor as shown below. Briefly, 1.0 g of ground sample was transferred to a 15 mL centrifuge tube containing 5 mL of methanol-borate buffer (1:1, *v*/*v*). After ultrasonic extraction for 15 min and centrifugation (8000 g, 4 °C) for 15 min, the separated supernatant was filtered through a 0.45 μm syringe filter. The filtrate was diluted with borate buffer (0.06 M, pH 7.8) containing 20 mM NaCl to yield sample solutions in 5% methanol before the analysis of OTA. To further assess the effectiveness of the developed method, four OTA-contaminated samples and one negative wheat sample were detected by the Nb-FRET immunosensor, and the results were validated by the LC-MS/MS method listed in the supplementary material (Liu et al., 2015).

3. Results and discussion

3.1 Characterization of OTA-GQDs and Nb-RQDs

Using the DCC/NHS method, OTA was covalently coupled with GQD-NH_2 for the preparation of OTA-GQDs. Under various reactant mole ratios of OTA to GQD-NH_2 (5:1, 10:1, 15:1, and 20:1), the binding rates of OTA were calculated to be 79.73%, 71.24%, 63.31% and 66.16%, which are equal to 3.98, 7.12, 9.49 and 13.23 molecules of OTA labeled on per GQD-NH_2 on average (Table S1). As seen in Fig. 1A, a redshift of the excitonic emission peak of OTA-GQDs was observed from 525 nm to 532 nm by comparison with that of GQD-NH_2. Moreover, the fluorescence intensity (λ_{ex}: 365 nm) of OTA-GQDs at 450 nm increased with the reactant mole ratio of OTA to GQD-NH_2, confirming the increasing amount of OTA chemically coupled on GQD-NH_2. However, the OTA-GQDs with the reactant mole ratio of 10:1 (OTA-GQDs-10) had the highest fluorescence intensity at 530 nm and the intensity decreased as the mole ratio exceeded 10. This could be attributed to the surface effect caused by excessive OTA immobilized on QDs, which may influence the change of its surface states from photoexcitation to photoemission (Hines and Kamat, 2014). FTIR analysis was conducted to validate the immobilization of OTA on the GQD-NH_2 (Fig. S1A and Table S2). The FTIR spectrum of GQD-NH_2 showed the N—H amide II characteristic peaks at 3436.90 cm^{-1} which were not observed in the spectrum of OTA-GQDs. In addition, the spectrum of OTA-GQDs exhibited the stretching vibrations of the C—N group at 1105.13 and 1359.72 cm^{-1} and the bending vibrations of the O—H group at 1438.79 cm^{-1}, respectively. These results indicate the successful immobilization of OTA on GQD-NH_2.

The anti-OTA Nb28 with high purity was confirmed by SDS-PAGE (Fig. S2) and subjected to the preparation of Nb-RQDs (Fig. 1B). Compared with the unlabeled RQD-COOH, the

fluorescence emission spectra of Nb-RQDs with different input mole ratios of Nb28 to RQD-COOH (2:1, 5:1, 10:1, and 20:1) all exhibited a single peak at 630 nm when excited at 525 nm. The coupling efficiencies were 71.07%, 81.69%, 66.12% and 59.06% for each group of Nb-RQDs (2:1, 5:1, 10:1 and 20:1). The group with the mole ratio of 5:1 (Nb-RQDs-5) showed the strongest fluorescence intensity at 630 nm in the spectra. The results correspond to 1.42, 4.08, 6.61 and 11.81 molecules of Nb28 immobilized on the RQD-COOH (Table S1). FTIR spectra of RQD-COOH and Nb-RQDs were compared (Fig. S1B and Table S3). Both RQD-COOH and Nb-RQDs showed amide bond characteristic peaks at 1643.23 cm^{-1} (C=O amide I). The free RQD-COOH also exhibited one special absorption band at 1070.42 cm^{-1} representing the C—O primary alcohol bond. Correspondingly, three peaks were recorded at 1103.20, 1359.72 and 1440.72 cm^{-1}, which stand for the stretching vibrations of the C—N group and the bending vibrations of the O—H group, respectively. These results could be attributed to the modified carboxyl group on RQD-COOH and thus demonstrate the successful covalent coupling between Nb28 and RQD-COOH.

3.2 Construction of the Nb-FRET immunosensor

The conjugation of OTA/Nb to QDs of two sizes made it accessible to act as donor and acceptor for constructing a FRET-based immunosensor. A checkerboard titration was designed to select the optimal mole ratio of OTA to GQD-NH_2 and of Nb28 to RQD-COOH (Table S4). Due to the stronger fluorescence intensity at 630 nm of Nb-RQDs-5 (λ_{ex}: 525 nm), both pairs of OTA-GQDs-5@Nb-RQDs-5 and OTA-GQDs-10@Nb-RQDs-5 exhibited higher energy transfer efficiency of 28.36% and 29.55% than the rest pairs. However, the efficiency of pairs of OTA-GQDs-15@Nb-RQDs-5 and OTA-GQDs-20@Nb-RQDs-5 was significantly decreased. This could be ascribed to the immobilization of excess OTA molecules on GQD-NH_2, which might enhance the hydrophobicity of QDs and thus hinder the specific binding between QDs in FRET through antigen–antibody interaction. Considering the result of titration, the pair of Nb-RQDs-5 (acceptor) and OTA-GQDs-10 (donor) was selected for the FRET system. The effective overlap between the fluorescence emission spectrum of donor and the molar extinction spectrum of acceptor is a prerequisite for FRET. As shown in Fig. 2A, the fluorescence emission spectrum of Nb-RQDs-5 overlapped well with the UV-vis absorption spectrum of OTA-GQDs-10. In addition, a good separation of emission spectra of Nb-RQDs-5 and OTA-GQDs-10 was observed. These results ascertain the occurrence of FRET from OTA-GQDs-10 to Nb-RQDs-5. TEM test was performed to confirm that the FRET was caused by the specific recognition of Nb-RQDs-5 to OTA-GQDs-10 (Fig. 2B). The mixture of GQD-NH_2 and RQD-COOH evenly dispersed in sight, whereas a number of aggregations of two, three and four QDs were observed in the mixture of OTA-GQDs-10 and Nb-RQDs-5. Thus the results indicate that the interaction between Nb and OTA triggered the FRET from OTA-GQDs-10 to Nb-RQDs-5.

3.3 Optimization of the Nb-FRET immunosensor

To obtain the optimal performance of the Nb-FRET immunosensor, a checkerboard titration for the mole ratio of Nb-RQDs-5 to OTA-GQDs-10 was firstly performed as shown in Table S5. The energy transfer efficiency increased from 23% to 34.49% with the mole ratio increasing from 1:1 to 4:1. In this situation, the higher concentration of Nb-RQDs-5 could facilitate more than one acceptor to react with the donor OTA-GQDs (shown in Fig. 2C) and

improve the overall energy transfer efficiency. However, the efficiency slightly decreased to 32.07% with the ratio reaching 5:1. It could be attributed to the excess Nb-RQDs-5 that may trigger an unpredictable fluorescence co-quenching phenomenon (Xu et al., 2014). Therefore, the mole ratio of 4:1 between the acceptor and donor was selected for further research.

Moreover, various assay conditions (reaction time, pH value, methanol concentration, ionic strength, and surfactant concentration) were optimized and the energy transfer efficiency was used for evaluation criterion. As shown in Fig. 3A, the energy transfer efficiency approached saturation after 5 min of incubation, and no significant variation was observed after further incubation. Thus, 5 min was selected as the optimal incubation time. When solution pH ranged from 6.8 to 7.8, the energy transfer efficiency dramatically increased from 22.33% to a maximum of 36.05%. Nevertheless, it rapidly decreased to 30.36% as the pH slightly increased to 8.0 (Fig. 3B). The results indicate that immunoreaction in the developed FRET system was highly sensitive to pH. Hence the recommended pH in assay buffer was 7.8. Methanol (MeOH) is generally used as the cosolvent of OTA in immunoassay and could influence the antigen-antibody interaction. Thus the performance of the Nb-FRET immunosensor under different MeOH concentrations was investigated. The FRET efficiency gradually increased from 30.07% to a maximum of 36.12% as the MeOH concentration did not exceed 5%. While a precipitous decline to 11.44% was observed as the MeOH concentration increased to 30% (Fig. 3C). Therefore, the selected final concentration of MeOH in assay buffer was 5%. To evaluate the effect of ionic strength on the Nb-FRET immunosensor, the borate buffers containing serial concentrations of sodium chloride (0, 10, 20, 50, 100 and 200 mM) were tested (Fig. 3D). The FRET efficiency reached a maximum of 38.28% as the NaCl concentration increased to 20 mM, whereas it significantly decreased with the further enhanced ionic strength. Therefore, 20 mM NaCl was selected as the optimal ionic strength in assay buffer. Furthermore, the assay buffers with various contents of nonionic surfactant Tween 20 were tested to reduce the nonspecific adsorption. But the result shown in Fig. 3E indicates that the addition of Tween 20 could significantly increase the standard deviations and reduce the FRET efficiency. To ensure the assay reliability and sensitivity, Tween 20 was not recommended for this proposed method. Thus, the optimal working conditions for the Nb-mediated FRET-based immunosensor were summarized as follows: acceptor and donor with the mole ratio of 4:1 were incubated in the borate buffer (0.06 M, pH 7.8) containing 5% MeOH and 20 mM NaCl for 5 min.

3.4 Analytical performance of the Nb-FRET immunosensor

Based on the optimal assay conditions, analytical performance of the Nb-FRET immunosensor was evaluated through the fluorescence spectra of the mixture of Nb-RQDs-5, OTA-GQDs-10, and serial concentrations of OTA (0, 0.005, 0.01, 0.02, 0.05, 0.1, 0.2, 0.5 and 1.0 ng/mL in borate buffer containing 50% MeOH, *v*/*v*) (Fig. 4A). The fluorescence intensity at 630 nm decreased as the OTA concentration increased. It confirms the competitive binding between OTA-GQDs-10 and OTA to Nb-RQDs-5, which could reduce the FRET efficiency. As shown in Fig. 4B, the energy transfer efficiency exhibited a good linear relationship with the logarithm of OTA concentration ranging from 0.005 to 1 ng/mL ($R^2 = 0.996$). The limit of detection (LOD) of the Nb-FRET immunosensor was

calculated to be 5 pg/mL, which is the lowest analyte concentration required to produce a signal greater than the 3-fold standard deviation of the noise level (S/N = 3). As a comparison, the mouse anti-OTA monoclonal antibody (mAb 6H8) was used to prepare the mAb 6H8-labeled RQDs (mAb-RQDs) for replacing the Nb-RQDs-5 (Fig. 4C). The mAb-RQDs with the input mole ratio of 2:1 between mAb 6H8 and RQD-COOH (mAb-RQDs-2) was selected as the acceptor together with the donor OTA-GQDs-10 for mAb-mediated FRET-based immunosensor (mAb-FRET immunosensor). Under the same experimental conditions, the mAb-FRET immunosensor had a linear range of 0.05–10 ng/mL and an LOD of 50 pg/mL, which is one order of magnitude higher than that of Nb-based system (Fig. 4D). Due to the tiny size of Nb, the utilization of Nb is an effective approach to shorten the effective FRET distance between donor and acceptor and thus increase the energy transfer efficiency and improve the detection limit of immunoassay. The selectivity of the Nb-FRET immunosensor for OTA was evaluated by determining the CR with two structural analogs of OTA (OTB and OTC) and four other cereal mycotoxins (AFB_1, ZEN, FB_1, and DON). As shown in Table S6, the immunosensor cross-reacted 4.56% with OTB, 30.33% with OTC, and less than 0.5% with AFB_1, ZEN, FB_1, and DON. These results indicate the good selectivity of the developed immunosensor for OTA. Moreover, an investigation of current immunosensors could provide deeper insight into the analytical performance of various biosensors and thus prove the superiority of this proposed ultrasensitive single-step Nb-FRET immunosensor (Table S7).

3.5 Detection of OTA in agro-products and validation

Since sample components in homogeneous methods are not removed by a wash step, the sample matrix could cause nonspecific binding and decrease the sensitivity. Thus the evaluation of the sample matrix effect is necessary prior to sample analysis, and the dilution method is generally used to reduce the matrix effect of food in immunoassays. As shown in Fig. S3, the matrix effect could be minimized after 10-, 25-, 40-, and 100-fold dilution of the extract of rice, barley, wheat, and oats, respectively. Accordingly, the final LODs of the developed immunosensor were 0.05 μg/kg in rice, 0.125 μg/kg in barley, 0.2 μg/kg in wheat, and 0.5 μg/kg in oats, respectively. The method sensitivity well meets the maximum limits of OTA in unprocessed cereal (5 μg/kg) and cereal products (3 μg/kg) set by the European Union (Commission of the European Communities, 2006). Based on the optimal dilution factors, the spiking and recovery experiments were performed to evaluate the effectiveness of the Nb-FRET immunosensor on cereal sample analysis. The negative cereal samples (rice, barley, wheat, and oats) with three spiking levels of OTA (0.02, 0.2 and 2 μg/kg) were pretreated and tested. As shown in Table S8, the average recovery rate and the relative standard deviation (RSD) of intra-assay ranged from 81% to 111% and from 3% to 9.4%, respectively. With respect to inter-assay, the average recovery rate and RSD were in the range of 80–109% and 4.5–9%, respectively. These results indicate the acceptable accuracy and precision of the Nb-FRET immunosensor. To further verify its reliability, nine OTA-contaminated samples (rice-1, -2, -4; oats-1, -2, -3; barley-1; wheat-1) and four negative samples (rice-3, oats-4, barley-2, wheat-2) were detected by the immunosensor, and the results were validated by the LC-MS/MS method as shown in Table 1. Thus, the Nb-FRET immunosensor is demonstrated to be applicable for rapid, ultrasensitive and selective detection of OTA in agro-products.

4. Conclusions

In this work, a novel FRET-based immunosensor using Nb and QDs was developed for quantitative analysis of ultra-trace OTA in cereal. The OTA and anti-OTA Nb were covalently coupled with QDs of two sizes, serving as the energy donor and acceptor, respectively. Compared with the traditional mAb, ease of expression of Nb in the prokaryotic system with high yield could contribute to reducing the cost. Moreover, the extremely small size of Nb made it more suitable for highly sensitive FRET-based immunoassay. Since the effective FRET distance between two QDs could be shortened using Nb, the FRET efficiency was accordingly improved for higher detection sensitivity. Due to the homogeneous detection system, the proposed method was also superior to both Nb- and mAb-based heterogeneous immunoassays for no-wash, single-step analysis with higher sensitivity. Thus, this study demonstrated that the Nbs have great application potential in FRET-based biosensing systems for detecting OTA and other small molecules in food and environment. To our knowledge, an Nb-mediated FRET-based immunosensor using QDs of two sizes for homogeneous and competitive detection of OTA and other low-molecular-weight compounds has not been reported yet.

Supplementary Material

Refer to Web version on PubMed Central for supplementary material.

Acknowledgements

This work was financially supported by the National Natural Science Foundation of China (grant number 31760493 and 31901800), the Natural Science Foundation of Hainan Province (grant number 219QN149), and the Scientific Research Foundation of Hainan University [grant number KYQD1631 and KYQD(ZR)1957]. We thank the approval of Analytical and Testing Center of Hainan University for the TEM and FTIR tests.

References

Bhatnagar D, Kumar V, Kumar A, Kaur I, 2016. Graphene quantum dots FRET based sensor for early detection of heart attack in human. Biosens. Bioelectron 79, 495–499. [PubMed: 26748366]

Binder EM, 2007. Managing the risk of mycotoxins in modern feed production. Anim. Feed Sci. Technol 133, 149–166.

Chen C, Cheng C, Lai C, Wu P, Wu K, Chou P, Chou Y, Chiu H, 2006. Potassium ion recognition by 15-crown-5 functionalized CdSe/ZnS quantum dots in H_2O. Chem. Commun. 3, 263–265.

Commission of the European Communities, 2006. Commission Regulation (EC) No. 1881/2006 of 19 December 2006 setting maximum levels for certain contaminants in foodstuffs. Off. J. Eur. Union L364, 5–24.

Damiano S, Navas L, Lombari P, Montagnaro S, Forte IM, Giordano A, Florio S, Ciarcia R, 2018. Effects of δ- tocotrienol on ochratoxin A-induced nephrotoxicity in rats. J. Cell. Physiol 233, 8731–8739. [PubMed: 29775204]

Dong B, Li H, Sun J, Mari GM, Yu X, Ke Y, Li J, Wang Z, Yu W, Wen K, Shen J, 2019. Development of a fluorescence immunoassay for highly sensitive detection of amantadine using the nanoassembly of carbon dots and MnO_2 nanosheets as the signal probe. Sensor. Actuat. B-Chem 286, 214–221.

Guo Y, Turnbull WB, Zhou D, 2018. Probing Multivalent Protein–Carbohydrate Interactions by Quantum Dot-Förster Resonance Energy Transfer, in: Imperiali B (Ed.), Methods in Enzymology. Academic Press, Elsevier Inc., Oxford, UK, pp. 71–100.

Harmsen MM, De Haard HJ, 2007. Properties, production, and applications of camelid single-domain antibody fragments. Appl. Microbiol. Biotechnol 77, 13–22. [PubMed: 17704915]

He J, Tian J, Xu J, Wang K, Li J, Gee SJ, Hammock BD, Li QX, Xu T, 2018. Strong and oriented conjugation of nanobodies onto magnetosomes for the development of a rapid immunomagnetic assay for the environmental detection of tetrabromobisphenol-A. Anal. Bioanal. Chem 410, 6633–6642. [PubMed: 30066195]

Heussner AH, Bingle LEH, 2015. Comparative ochratoxin toxicity: A review of the available data. Toxins 7, 4253–4282. [PubMed: 26506387]

Hines DA, Kamat PV, 2014. Recent advances in quantum dot surface chemistry. ACS Appl. Mater. Inter 6, 3041–3057.

International Agency for Research on Cancer (IARC), 1993. Some Naturally Occurring Substances: Food Items and Constituents, Heterocyclic Aromatic Amines and Mycotoxins, in: IARC Monographs on the Evaluation of the Carcinogenic Risk of Chemicals to Humans. World Health Organization, IARC, Lyon, France, Vol. 56.

Jo EJ, Mun H, Kim MG, 2016. Homogeneous immunosensor based on luminescence resonance energy transfer for glycated hemoglobin detection using upconversion nanoparticles. Anal. Chem 88, 2742–2746. [PubMed: 26836651]

Lakowicz JR, 1999. Instrumentation for Fluorescence Spectroscopy, Principles of Fluorescence Spectroscopy. Springer US, Boston, MA, pp. 25–61.

Liu X, Tang Z, Duan Z, He Z, Shu M, Wang X, Gee SJ, Hammock BD, Xu Y, 2017. Nanobody-based enzyme immunoassay for ochratoxin A in cereal with high resistance to matrix interference. Talanta 164, 154–158. [PubMed: 28107910]

Liu X, Xu Y, Wan D, Xiong Y, He Z, Wang X, Gee SJ, Dojin R, Hammock BD, 2015. Development of a nanobody–alkaline phosphatase fusion protein and its application in a highly sensitive direct competitive fluorescence enzyme immunoassay for detection of ochratoxin A in cereal. Anal. Chem 87, 1387–1394. [PubMed: 25531426]

Liu X, Xu Y, Xiong Y, Tu Z, Li Y, He Z, Qiu Y, Fu J, Gee SJ, Hammock BD, 2014. VHH phage-based competitive real-time immuno-polymerase chain reaction for ultrasensitive detection of ochratoxin A in cereal. Anal. Chem 86, 7471–7477. [PubMed: 24992514]

Masters BR, 2014. Paths to Förster's resonance energy transfer (FRET) theory. Eur. Phys. J. H 39, 87–139.

Muyldermans S, 2013. Nanobodies: natural single-domain antibodies. Annu. Rev. Biochem 82, 775–797. [PubMed: 23495938]

Nelson AL, 2010. Antibody fragments: hope and hype. mAbs 2, 77–83. [PubMed: 20093855]

Nsibande SA, Forbes PBC, 2016. Fluorescence detection of pesticides using quantum dot materials–a review. Anal. Chim. Acta 945, 9–22. [PubMed: 27968720]

Öncü Kaya EM, Korkmaz OT, Yeniceli Uğur D, Şener E, Tunçel AN, Tunçel M, 2019. Determination of Ochratoxin-A in the brain microdialysates and plasma of awake, freely moving rats using ultra high performance liquid chromatography fluorescence detection method. J. Chromatogr. B 1125, 121700.

Pagkali V, Petrou PS, Makarona E, Peters J, Haasnoot W, Jobst G, Moser I, Gajos K, Budkowski A, Economou A, Misiakos K, Raptis I, Kakabakos SE, 2018. Simultaneous determination of aflatoxin B_1, fumonisin B_1 and deoxynivalenol in beer samples with a label-free monolithically integrated optoelectronic biosensor. J. Hazard. Mater 359, 445–453. [PubMed: 30059886]

Pagkali V, Petrou PS, Salapatas A, Makarona E, Peters J, Haasnoot W, Jobst G, Economou A, Misiakos K, Raptis I, Kakabakos SE, 2017. Detection of ochratoxin A in beer samples with a label-free monolithically integrated optoelectronic biosensor. J. Hazard. Mater 323, 75–83. [PubMed: 26988901]

Qian Y, Fan T, Wang P, Zhang X, Luo J, Zhou F, Yao Y, Liao X, Li Y, Gao F, 2017. A novel label-free homogeneous electrochemical immunosensor based on proximity hybridization-triggered isothermal exponential amplification induced G-quadruplex formation. Sensor. Actuat. B-Chem 248, 187–194.

Qiu X, Wegner KD, Wu Y, van Bergen en Henegouwen PMP, Jennings TL, Hildebrandt N, 2016. Nanobodies and antibodies for duplexed EGFR/HER2 immunoassays using terbium-to-quantum dot FRET. Chem. Mater 28, 8256–8267.

Qiu Y, Li P, Dong S, Zhang X, Yang Q, Wang Y, Ge J, Hammock BD, Zhang C, Liu X, 2018. Phage-mediated competitive chemiluminescent immunoassay for detecting Cry1Ab toxin by using an anti-idiotypic camel nanobody. J. Agric. Food Chem 66, 950–956. [PubMed: 29293334]

Ren W, Li Z, Xu Y, Wan D, Barnych B, Li Y, Tu Z, He Q, Fu J, Hammock BD, 2019. One-step ultrasensitive bioluminescent enzyme immunoassay based on nanobody/nanoluciferase fusion for detection of aflatoxin B_1 in cereal. J. Agric. Food Chem 67, 5221–5229. [PubMed: 30883117]

Rodríguez-Cabo T, Rodríguez I, Ramil M, Cela R, 2016. Liquid chromatography quadrupole time-of-flight mass spectrometry selective determination of ochratoxin A in wine. Food Chem 199, 401–408. [PubMed: 26775988]

Shin HS, Lee HJ, Pyo MC, Ryu D, Lee KW, 2019. Ochratoxin A-induced hepatotoxicity through phase I and phase II reactions regulated by AhR in liver cells. Toxins 11, 377.

Stoev SD, 2010. Studies on carcinogenic and toxic effects of ochratoxin A in chicks. Toxins 2, 649–664. [PubMed: 22069604]

Sun Z, Duan Z, Liu X, Deng X, Tang Z, 2017. Development of a nanobody-based competitive dot ELISA for visual screening of Ochratoxin A in cereals. Food Anal. Method. 10, 3558–3564.

Sun Z, Lv J, Liu X, Tang Z, Wang X, Xu Y, Hammock BD, 2018. Development of a nanobody-aviTag fusion protein and its application in a streptavidin–biotin-amplified enzyme-linked immunosorbent assay for ochratoxin A in cereal. Anal. Chem 90, 10628–10634. [PubMed: 30092629]

Sun Z, Wang X, Tang Z, Chen Q, Liu X, 2019. Development of a biotin-streptavidin-amplified nanobody-based ELISA for ochratoxin A in cereal. Ecotox. Environ. Safe 171, 382–388.

Takkinen K, Žvirblienė A, 2019. Recent advances in homogenous immunoassays based on resonance energy transfer. Curr. Opin. Biotechnol 55, 16–22. [PubMed: 30075375]

Tang Z, Liu X, Wang Y, Chen Q, Hammock BD, Xu Y, 2019. Nanobody-based fluorescence resonance energy transfer immunoassay for noncompetitive and simultaneous detection of ochratoxin A and ochratoxin B. Environ. Pollut 251, 238–245. [PubMed: 31082608]

Tang Z, Wang X, Lv J, Hu X, Liu X, 2018. One-step detection of ochratoxin A in cereal by dot immunoassay using a nanobody-alkaline phosphatase fusion protein. Food Control 92, 430–436.

Tu Z, Chen Q, Li Y, Xiong Y, Xu Y, Hu N, Tao Y, 2016. Identification and characterization of species-specific nanobodies for the detection of Listeria monocytogenes in milk. Anal. Biochem 493, 1–7. [PubMed: 26456330]

Ullman EF, 2013. Homogeneous immunoassay, in: Wild D (Ed.), The Immunoassay Handbook: Theory and applications of ligand binding, ELISA and related techniques. Elsevier Ltd., Oxford, UK, pp. 67–87.

Vinayaka AC, Thakur MS, 2013. Facile synthesis and photophysical characterization of luminescent CdTe quantum dots for Forster resonance energy transfer based immunosensing of staphylococcal enterotoxin B. Luminescence 28, 827–835. [PubMed: 23192990]

Vincke C, Muyldermans S, 2012. Introduction to Heavy Chain Antibodies and Derived Nanobodies, in: Saerens D, Muyldermans S (Eds.), Single Domain Antibodies: Methods and Protocols. Humana Press, Totowa, NJ, pp. 15–26.

Wang J, Bever CRS, Majkova Z, Dechant JE, Yang J, Gee SJ, Xu T, Hammock BD, 2014. Heterologous antigen selection of camelid heavy chain single domain antibodies against tetrabromobisphenol A. Anal. Chem 86, 8296–8302. [PubMed: 25068372]

Wang J, Majkova Z, Bever CRS, Yang J, Gee SJ, Li J, Xu T, Hammock BD, 2015. One-step immunoassay for Tetrabromobisphenol A using a camelid single domain antibody–alkaline phosphatase fusion protein. Anal. Chem 87, 4741–4748. [PubMed: 25849972]

Wang K, Liu Z, Ding G, Li J, Vasylieva N, Li QX, Li D, Gee SJ, Hammock BD, Xu T, 2019a. Development of a one-step immunoassay for triazophos using camel single-domain antibody–alkaline phosphatase fusion protein. Anal. Bioanal. Chem 411, 1287–1295. [PubMed: 30706076]

Wang K, Vasylieva N, Wan D, Eads DA, Yang J, Tretten T, Barnych B, Li J, Li QX, Gee SJ, Hammock BD, Xu T, 2019b. Quantitative detection of fipronil and fipronil-sulfone in sera of black-tailed prairie dogs and rats after oral exposure to fipronil by camel single-domain antibody-based immunoassays. Anal. Chem 91, 1532–1540. [PubMed: 30521755]

Wei D, Wu X, Xu J, Dong F, Liu X, Zheng Y, Ji M, 2018. Determination of Ochratoxin A contamination in grapes, processed grape products and animal-derived products using ultra-

performance liquid chromatography-tandem mass spectroscopy system. Sci. Rep 8, 2051. [PubMed: 29391603]

Woo CSJ, Partanen H, Myllynen P, Vähäkangas K, El-Nezami H, 2012. Fate of the teratogenic and carcinogenic ochratoxin A in human perfused placenta. Toxicol. Lett 208, 92–99. [PubMed: 22037670]

Xu Q, Liu Y, Su R, Cai L, Li B, Zhang Y, Zhang L, Wang Y, Wang Y, Li N, Gong X, Gu Z, Chen Y, Tan Y, Dong C, Sreeprasad TS, 2016. Highly fluorescent Zn-doped carbon dots as Fenton reaction-based bio-sensors: an integrative experimental–theoretical consideration. Nanoscale 8, 17919–17927. [PubMed: 27725980]

Xu W, Xiong Y, Lai W, Xu Y, Li C, Xie M, 2014. A homogeneous immunosensor for AFB_1 detection based on FRET between different-sized quantum dots. Biosens. Bioelectron 56, 144–150. [PubMed: 24487101]

Zangheri M, Cevenini L, Anfossi L, Baggiani C, Simoni P, Di Nardo F, Roda A, 2015. A simple and compact smartphone accessory for quantitative chemiluminescence-based lateral flow immunoassay for salivary cortisol detection. Biosens. Bioelectron 64, 63–68. [PubMed: 25194797]

Zhang X, Li M, Cheng Z, Ma L, Zhao L, Li J, 2019. A comparison of electronic nose and gas chromatography–mass spectrometry on discrimination and prediction of ochratoxin A content in Aspergillus carbonarius cultured grape-based medium. Food Chem 297, 124850. [PubMed: 31253256]

Zhou R, Sun S, Li C, Wu L, Hou X, Wu P, 2018. Enriching Mn-doped ZnSe quantum dots onto mesoporous silica nanoparticles for enhanced fluorescence/magnetic resonance imaging dual-modal bio-imaging. ACS Appl. Mater. Inter 10, 34060–34067.

Highlights

- A nanobody-mediated immunosensor based on FRET between different-sized QDs for OTA
- The nanobody shortens the effective FRET distance for higher detection sensitivity
- OTA is determined following a competitive and homogeneous immunoassay format
- The assay could be finished in 5 min with a detection limit of 5 pg/mL for OTA
- The immunosensor is applicable for rapid screening of OTA in agro-products

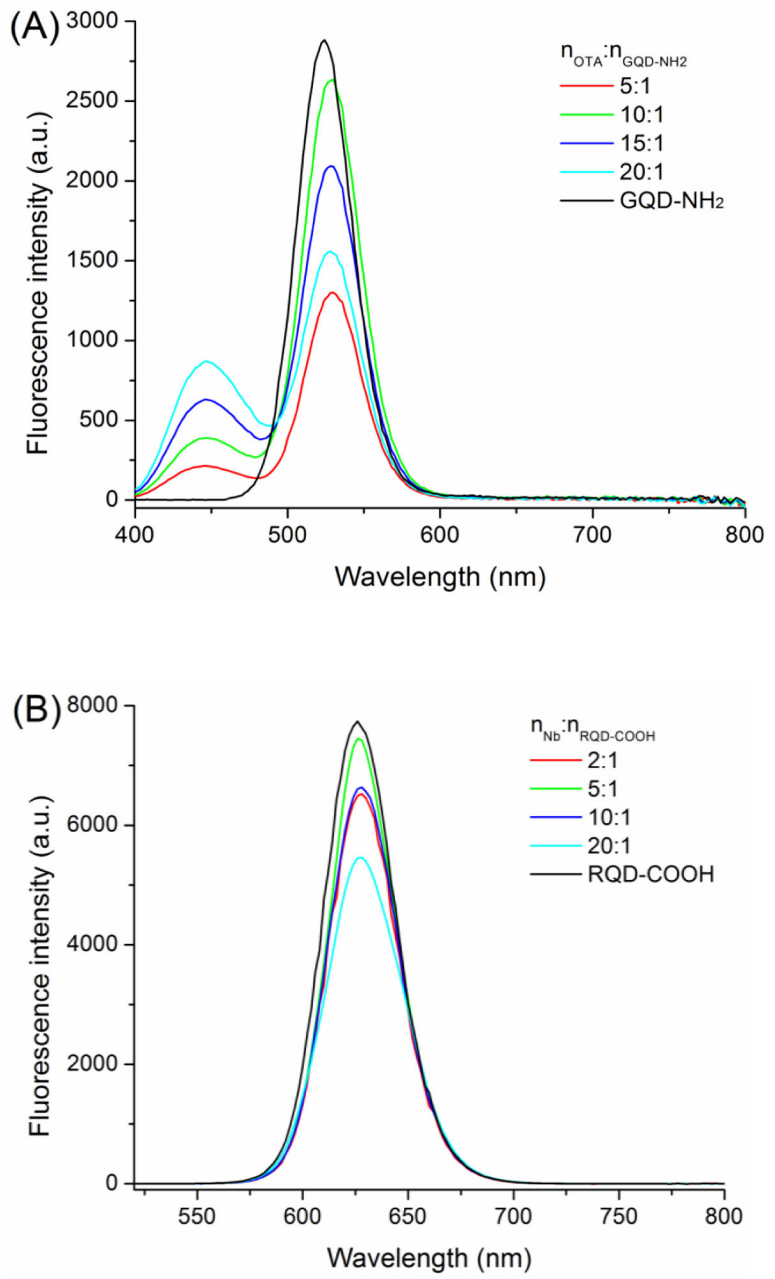

Fig. 1.

Fluorescence emission spectra (λ_{ex}: 425 nm) of different mole ratios (5:1, 10:1, 15:1, 20:1) of OTA to GQD-NH_2 (A) and fluorescence emission spectra (λ_{ex}: 530 nm) of different mole ratios (2:1, 5:1, 10:1, 20:1) of Nb28 to RQD-COOH (B).

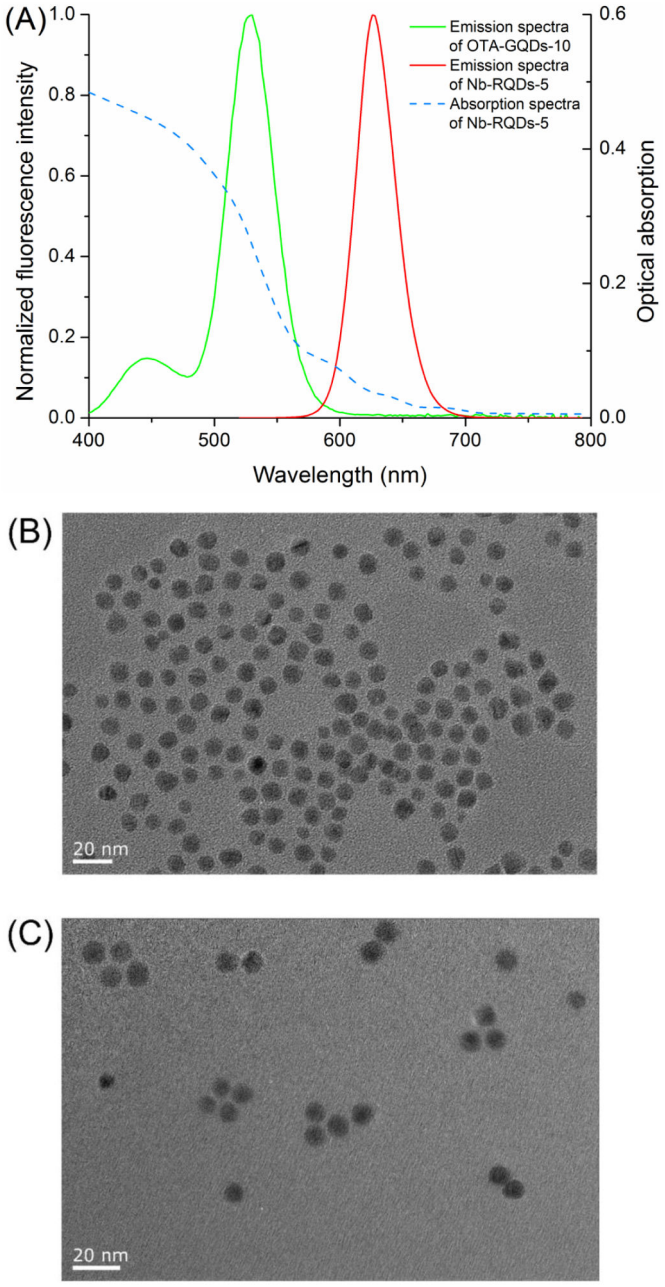

Fig. 2.

(A) The fluorescence emission spectra of OTA-GQD-10 (λ_{ex}: 425 nm) and Nb-RQD-5 (λ_{ex}: 530 nm) and the UV absorption spectra of OTA-GQD-10. The TEM analysis of the mixture of GQD-NH_2 and RQD-COOH (B) and the mixture of OTA-GQDs-10 and Nb-RQDs-5 (C).

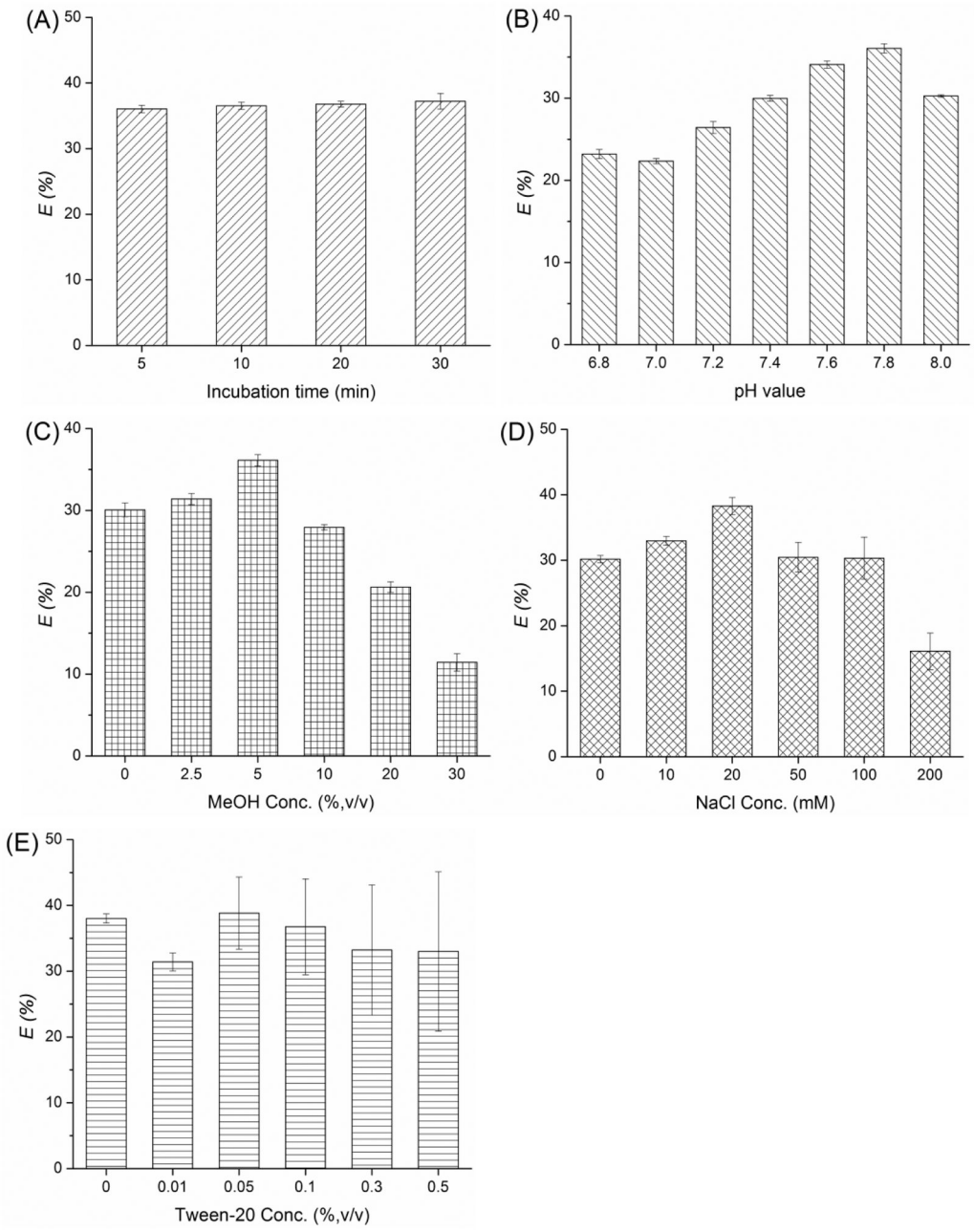

Fig. 3.

The effects of immunoreaction time (A), pH value (B), methanol concentration (C), ionic strength (D), and Tween-20 concentration (E) on the energy transfer efficiency of the Nb-FRET immunosensor. Error bars indicate standard deviations of data from experiments performed in triplicate.

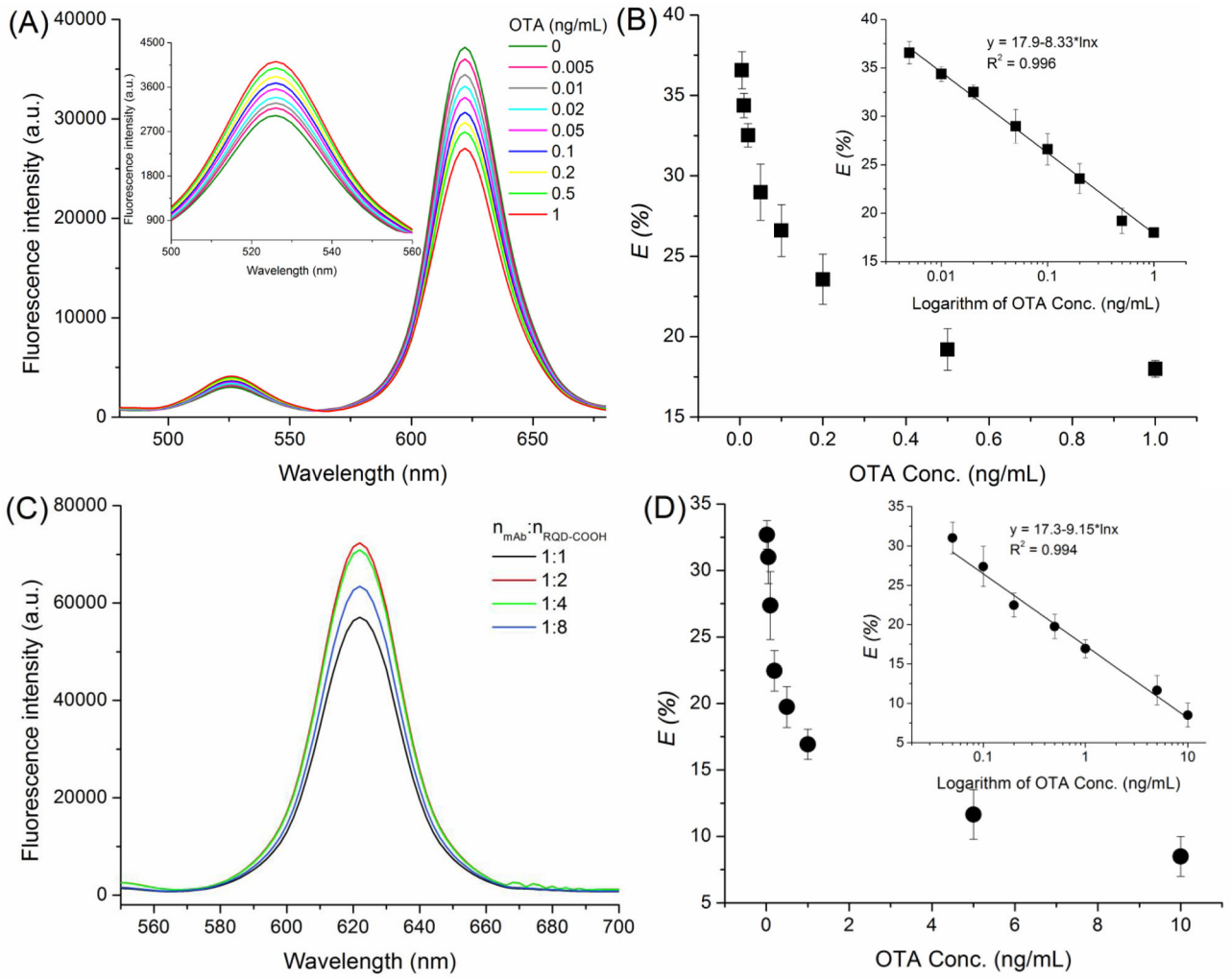

Fig. 4.

Fluorescence emission spectra of the mixture of OTA-GQD-10 and Nb-RQD-5 with various concentrations of OTA (A), and the plot of the energy transfer efficiency against the logarithm of OTA concentrations (B). Fluorescence emission spectra (λ_{ex}: 530 nm) of different mole ratios of OTA-specific mAb to RQD-COOH (C) and plot of the energy transfer efficiency against the logarithm of OTA concentrations (D). The fluorescence spectra were recorded with excitation at 425 nm. Inset in: the linear portion of the plot. The error bars indicate standard deviations of data from experiments performed in triplicate.

Table 1.

Determination of OTA content in cereal samples.

Sample	LC-MS/MS[a] (μg/kg)	Nb-FRET immunosensor (μg/kg)
rice-1	2.03 ± 0.09	1.45 ± 0.08
rice-2	1.80 ± 0.17	1.68 ± 0.13
rice-3	ND[b]	ND
rice-4	1.45 ± 0.18	1.58 ± 0.15
oats-1	0.82 ± 0.10	0.89 ± 0.07
oats-2	7.53 ± 0.11	8.63 ± 0.95
oats-3	12.0 ± 0.30	13.8 ± 0.90
oats-4	ND	ND
oats-5	1.22 ± 0.04	1.34 ± 0.10
barley-1	1.83 ± 0.14	1.64 ± 0.11
barley-2	ND	ND
wheat-1	ND	0.006 ± 0.00006
wheat-2	ND	ND

[a]The LOD of the LC-MS/MS method is 0.01 ng/mL (Liu et al., 2015).

[b]Not detected.